NASA Technical Memorandum 105172

Ground-Based PIV and Numerical Flow Visualization Results From the Surface Tension Driven Convection Experiment

Alexander D. Pline and Mark P. Wernet
National Aeronautics and Space Administration
Lewis Research Center
Cleveland, Ohio

and

Kwang-Chung Hsieh
Sverdrup Technology, Inc.
Lewis Research Center Group
Brook Park, Ohio

Prepared for the
36th Annual International Symposium on Optical and
Optoelectronic Applied Science and Engineering
sponsored by the Society of Photo-Optical Instrumentation Engineers
San Diego, California, July 21–26, 1991

NASA

Ground-Based PIV and Numerical Flow Visualization Results From the Surface Tension Driven Convection Experiment

Alexander D. Pline and Mark P. Wernet
National Aeronautics and Space Administration
Lewis Research Center
Cleveland, Ohio 44135

Kwang-Chung Hsieh
Sverdrup Technology, Inc.
Lewis Research Center Group
Brook Park, Ohio 44142

ABSTRACT

The Surface Tension Driven Convection Experiment (STDCE) is a Space Transportation System flight experiment to study both transient and steady thermocapillary fluid flows aboard the USML—1 Spacelab mission planned for June, 1992. One of the components of data collected during the experiment is a video record of the flow field. This qualitative data is then quantified using an all electronic, two dimensional Particle Image Velocimetry (PIV) technique called Particle Displacement Tracking (PDT) which uses a simple space domain particle tracking algorithm. Results using the ground—based STDCE hardware, with a radiant flux heating mode, and the PDT system are compared to numerical solutions obtained by solving the axisymmetric Navier Stokes equations with a deformable free surface. The PDT technique is successful in producing a velocity vector field and corresponding stream function from the raw video data which satisfactorily represents the physical flow. A numerical program is used to compute the velocity vector field and corresponding stream function under identical conditions. Both the PDT system and numerical results were compared to a streak photograph, used as a benchmark, with good correlation.

1. INTRODUCTION

The Surface Tension Driven Convection Experiment (STDCE) is a fluid physics experiment to determine the nature and extent of transient and steady thermocapillary flows in the reduced gravity environment of low earth orbit aboard the Space Shuttle. The STDCE is manifested for flight on the United States Microgravity Laboratory—1 Space Shuttle mission, planned for 1992. Thermocapillary flow, or surface tension driven flow, is generated by a thermally induced surface tension variation along a liquid—gas free surface. The surface tension gradient, established by non—uniform heating the free surface, is a surface tractive force, which creates a flow parallel to the liquid—gas interface from regions of low surface tension to high surface tension. Thermocapillary flows are important in technological applications where free surfaces are inherent and gravitational forces are small compared to capillary forces[1], such as containerless processing and crystal growth in low gravity, and terrestrial welding. Under certain circumstances periodic flow oscillations can occur[2-3] which are considered to be detrimental to the above processes.

In order to quantitatively study the STDCE flow field a flow velocity measurement technique was sought. Requirements imposed by both the Experiment Investigators S. Ostrach and Y. Kamotani, of Case Western Reserve University, and the Shuttle on—board operating constraints have dictated the use of this particular measurement technique and data reduction system. The STDCE requires continuous recording of the qualitative flow patterns so that the evolution of the flow field with time can be studied. In addition, a method to quantify the qualitative record is required. The axisymmetric nature of the STDCE steady flow, studied in this flight, greatly simplifies the task of quantitative study. On—board operation of the experiment dictates the use of a convenient, low volume storage technique and ease of operation. Based on these requirements, an all electronic Particle Image Velocimetry (PIV) technique, recording light scattered from small seed particles following the flow on video tape, is well suited for this application.

Many of the techniques available for acquiring, storing and reducing PIV data utilize traditional photographic recordings and sophisticated processing hardware. They are also difficult to set up, are time consuming and expensive.[4-6] The PDT technique is an all electronic technique which employs a single large memory buffer frame—grabber board to digitize PIV images from an RS—170 video source (i.e. flow data imaged using a CCD video camera and recorded on a shuttle videocasette recorder). In the PDT technique, a sequence of images are time coded into a single binary file using a simple encoding scheme and then processed to track particle displacements and determine velocity vectors. All of the data acquisition reduction and analysis is performed on a 80386 PC, no array processors or other specialized processing hardware are required.

In a previous paper[8] a single data set was presented to demonstrate the detailed workings of the PDT algorithms and operation to show feasibility of using the PDT system for the STDCE. In this paper the PDT system was used to acquire and reduce flow visualization data from a ground—based laboratory mock—up of the STDCE, further demonstrating the ability of the PDT system to adequately quantify the qualitative flow fields recorded during the STDCE. The flow data were acquired during steady state conditions using the STDCE constant flux boundary condition, consisting of a temperature gradient created by imposing a Gaussian heat flux distribution on the free surface. The heat flux distribution shape and total power were set as experimental conditions. Also, a numerical code was previously written as an additional tool for studying the STDCE flow field.[10] The code solves the Navier Stokes equations with the Boussinesq approximation for the axisymmetric STDCE geometry with both the constant flux boundary condition and other boundary conditions studied during the STDCE. The flow field was computed under the same conditions as the experimental data. Both the PDT system data and the numerical calculation were compared to a streak photograph, which was used as a benchmark as it was a direct record of the actual event. The comparison of the three techniques is an independent check for both the PDT system and the numerical code.

2. EXPERIMENTAL AND NUMERICAL TECHNIQUES

2.1. Particle Displacement Tracking system

The Particle Displacement Tracking (PDT) system uses an EPIX 4—MEG video frame—grabber board to digitize and store PIV images from any RS—170 video source, either camera or VCR. The frame—grabber board is equipped with a 12.5 MHz A/D oscillator so that interlaced 640×480 square pixel frames are digitized. The frame—grabber board is configured to digitize individual fields with a minimum sampling time of 1/60 second. However, by using just fields, the vertical resolution is halved, producing a 640 pixel × 240 line image from the even or odd fields from the RS—170 interlaced video signal. The reduced vertical sampling is not a significant effect if the particle images encompass several pixels across their diameters. When acquiring video fields, 25 fields are acquired and stored in the 4 Mbyte on—board memory buffer.

The PDT system is applicable only to low velocity ($\lesssim$ 20 cm/s), sparsely seeded PIV fluid flow systems. In the PDT system, a cw laser source is used to generate a light sheet, and a video array camera/frame—grabber board records the particle image data. The frame—grabber board is used to acquire five video fields equally spaced in time from the RS—170 video source. The choice of five fields minimizes the error rate in subsequent processing.[9] The time interval, ΔT, between recorded fields is 1/60 second at the minimum, and essentially unlimited at the maximum time interval which corresponds to the minimum velocities. The actual value of ΔT is selected according to the fluid velocities of interest. The particle seeding number density is selected so that the individual particles are clearly imaged.

The five video fields are then individually processed to determine the centroid location of each particle image on each video field in the sequence. The particle centroid information is sufficient to determine the displacement of the particles between fields. A simple boundary following algorithm is used to identify the individual particle images. Each particle image centroid is computed using the particle image light intensity distribution. The particle image amplitude and shape information are used in estimating the centroids and subsequently discarded. The particle image centroids are determined to within $\pm \frac{1}{2}$ pixel.

The single pixel particle centroid estimates from each of the particle images recorded in the five—field sequence are combined into a single 640×480×8 bit pixel binary file. The time history of each particle image is encoded in the amplitude of the pixel marking the position of the particle centroid, with the pixel amplitudes coded according to the time order in the five field sequence. All of the particle centroids from video field #1 are encoded into the composite binary file as pixels with amplitudes 2^1. Similarly, particle centroids from video field #2 are encoded with amplitude 2^2, etc. By amplitude coding the pixel locations of the particle centroids, a 2—D array is generated which contains the time history displacements of all the particles recorded in the five field sequence over a total time interval of $4\Delta T$. Amplitude coding unambiguously defines the particle's direction of travel. The amplitude coding also decreases the probability of mistakenly identifying a particle image from a different particle as being part of another particle displacement record. Another advantage of using single exposure particle images fields is the elimination of particle image overlap, which typically restricts the lower limit of velocities which can be measured with techniques utilizing traditional multi—exposure photographic techniques. By individually processing the video image fields, particle images, in each field, with large diameters relative to their displacement between exposures are easily tolerated. The only constraint on the minimum velocity is that the particle must travel at least one pixel between video fields.

The time history file serves as the input to the PDT algorithm which begins by scanning the time history file and storing the locations of all pixels with amplitude 2^1, which correspond to all particle positions at the initial field in the sequence, and serve as the starting point for the displacement tracking. By determining the displacement of the particle from its initial position, the velocity information of the flow is inferred.

For each initial particle position, a circular search region is defined around the 2^1 amplitude pixel. Inside the search region, the coordinates of all pixels with amplitudes equal to 2^2 are stored. The 2^2 amplitude coded pixels correspond to the particle positions at $1\Delta T$, or field #2. The detected 2^2 amplitude pixels within the search region are now each successively analyzed. The distance and angle between each 2^2 amplitude pixel and the search region center 2^1 amplitude pixel is computed and used to project where the 2^3, 2^4, and 2^5 amplitude pixels are located which correspond to the 2^1 and 2^2 amplitude pixel particles (Figure 1). If the projected pixel

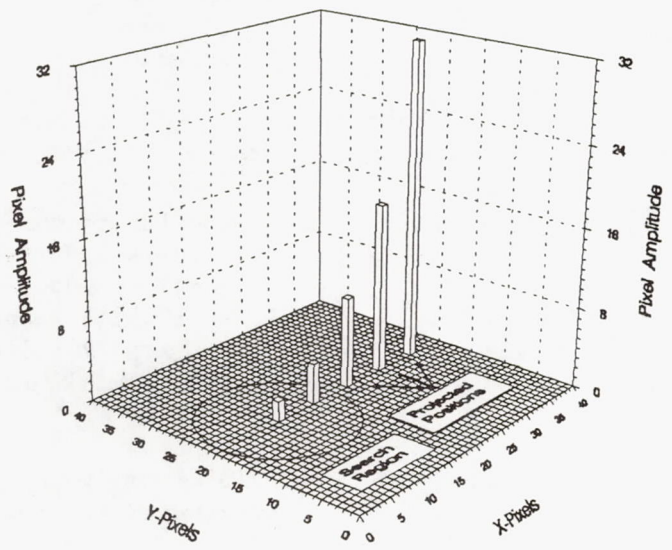

Figure 1. PDT technique determining velocity vectors by defining a circular search region around each 2^1 amplitude pixel. All 2^2 amplitude pixels within the search region are detected. The distance and angle from the 2^1 amplitude pixel and all detected 2^2 amplitude pixels are used to project where the subsequent third, fourth, and fifth pixel video field particle images will occur. The projected 3×3 pixel search regions are indicated.

locations for the 3rd, 4th, and 5th particle images contain the corresponding amplitudes (2^3, 2^4, 2^5) then a complete particle displacement record has been detected. The velocity vector associated with this particle is computed from the distance between the initial and final particle locations (2^1 and 2^5 amplitude pixels), and the sum of the four inter—field times (IFT), $4\Delta T$. The detected particle pixel amplitudes are then set to zero to avoid confusion in subsequent searches.

If the incorrect pixel amplitude or zero amplitude is detected at the projected particle locations, then the 2^2 amplitude pixel within the search region is not considered the actual second image of the 2^1 amplitude pixel at the center of the search region. Each 2^2 amplitude pixel within the search region is examined until a complete particle displacement pattern is detected or all of the 2^2 amplitude pixels are exhausted. If no match is found, the algorithm continues on to the next initial particle position 2^1 amplitude pixel. As a result of the technique no preknowledge about the flow system is required. The PDT system assumes that 2^2 amplitude pixels in the neighborhood of the initial 2^1 amplitude pixel are the most probable particle displacements between video fields #1 and #2 in the five field sequence. The maximum allowable particle displacement between fields has previously been determined to be 10 pixels for sharply turning flows.[9] Ten pixel displacements between fields minimizes the deviation of the particle path from a linear trajectory. Therefore, the search region size is defined to be a circle of radius 10 pixels (Figure 1).

The random locations of independent particle images on the time history image frame can be misconstrued as originating from a single particle, which results in a false velocity vector identification. The main factor affecting the number of false identifications is the particle density in the fluid. The number of false identifications is greatly reduced by using the above described particle time history information. A thorough analysis of the expected number of false identifications is presented in Reference 8.

The positioning error on the discrete grid must be accommodated in the PDT processing. As previously mentioned, the boundary processing technique provides particle centroid estimates to within $\pm \frac{1}{2}$ pixel on the 640×480 pixel time history image. For each projected particle position (for exposures 3, 4, 5) a 3×3 pixel search region is defined. The 3×3 search regions are centered on the projected positions (Figure 1), allowing for the positioning error of $\pm \frac{1}{2}$ pixel. However, when a complete particle displacement pattern is detected, the exact location of the amplitude coded pixel within the 3×3 region is used to determine the velocity vector magnitude. The velocity vector angle is computed from the position of the 2^1 and 2^5 amplitude pixels.

There are two sources of error in the PDT estimated velocities: 1) the particle positioning error; and 2) the time interval error. The time interval error is minimal since the frame—grabber board is genlocked to the RS—170 video signal from the video camera. The major source of error is from the particle centroid estimates. Typical total relative errors in measured velocity magnitude and direction are[8-9]:

1.8% and 1.0° for maximum velocities and

18% and 10.0° for minimum velocities.

A unique feature of the PDT technique is afforded by the use of a large memory buffer frame—grabber board to store 25 sequentially acquired video fields. The 25 fields are grouped in successive sets of 5 fields and processed by the PDT technique described above. The five groups of 5 successive fields produce five 2—D velocity vector maps. Particles may be tracked across all five groups, for all 25 fields. Hence, the composite 2—D velocity vector map may track particles for all five sampling intervals. Particles tracked for all 25 fields will be represented by a string of velocity vectors oriented head to tail, which indicates the particle path over the total measurement time of $24\Delta T$.

The data acquisition and PDT processing are all performed on a 33 MHz 80386 computer with a Weitek 3167 coprocessor. All of the PDT processing routines are written in Fortran 77 and compiled with a 32 bit Weitek supported compiler.

The data acquisition software prompts the user for the number of video fields to elapse between the acquired video fields. For low velocity flows many video fields are allowed to elapse between successively acquired images. For faster flows, adjacent fields can be acquired resulting in the minimum ΔT of 1/60 second. The coordinates obtained from the reservoir boundary are used to delimit the region of the image to be processed to determine particle image centroids. Stray sources of light outside the reservoir are ignored by defining the reservoir as a subregion of the recorded image. The threshold level, determined using the data acquisition software is used in the centroid processing program to eliminate background noise in the recorded image, because

the centroid processing algorithm requires that the particle images be distinctly defined, i.e. zero level is assigned between particle images.

Data sets sampled with different IFTs are combined and plotted to produce graphs with high dynamic range. An algorithm to remove falsely identified velocity vectors from the data sets is used before plotting. Typically, a few percent of the velocity vectors obtained will be falsely identified velocity vectors[8]. The main premise used in the irregular vector removal algorithm is that there are a sufficient number of 'good' velocity vectors surrounding the 'bad' velocity vectors. The mean 'good' qualities are used to attempt to eliminate the falsely identified velocity vectors.

A routine interpolates the randomly sampled data to a regular grid pattern (selectable up to 148×148) by sorting the velocity vector data, finding the 20 nearest neighbors to the grid point being computed and performing a linear least squares interpolation to estimate the velocity at the grid point. The stream function of the flow is then computed using this interpolated velocity vector information. A more complete description of the PDT system hardware and software can be found in Reference 11.

Also included as an independent check of the qualitative flow patterns produced by the PDT hardware and software were comparison to streak photographs made using a 35 mm SLR camera with a long time exposure (seconds) under identical experimental conditions.

2.2. Numerical calculations

To obtain an additional tool for studying the Surface Tension Driven Convection Experiment flow with a deformable free surface, a program with a high—order accuracy has been developed. The governing equations are formulated based on the three dimensional Navier Stokes equations with the Boussinesq approximation, coupled with species transport equations. Although the model is based on the three dimensional equations the code is currently axisymmetric limited. The absorption of the laser radiation is accounted for by including a measured absorption coefficient and a Gaussian distribution along the free surface. In order to incorporate the effect of free surface deformation, the equations are transformed using generalized dynamic coordinates. The governing equations are solved using a numerical technique in which the divergence—free condition is achieved by using a dual time—stepping approach.[10] The flow equations, cast in pseudotime τ, are in hyperbolic form with the aid of artificial compressibility and are integrated in τ until convergence for each physical time step.

Convective flux differences are evaluated using third—order—accurate upwind—biased flux—split differencing.[10] The implicit operators generated using upwind fluxes are diagonally dominant and have good stability and convergence characteristics. The numerical grid is 62×123 with the grid points clustered near the centerline and boundaries to provide good resolution in the boundary layer regions. The code has been written in multiple block fashion for complicated geometry and in time—dependent generalized coordinates for free surface deformation. The detailed equations and appropriate boundary conditions can be found in Reference 10.

3. EXPERIMENTAL SETUP AND TECHNIQUE

3.1. Experimental set—up

The ground—based development mock—up of the STDCE is shown in Figure 2. The test chamber consists of a 10 cm diameter by 5 cm deep hole bored into a 12.7 cm square by 6.4 cm high plexiglas block. Plexiglas was chosen to provide good optical access to the chamber. In the flight hardware configuration a copper wall is used to maintain a more well defined wall thermal boundary condition, at the expense of easy optical access, requiring a non—linear coordinate transformation to correct for optical distortions[8]. The heat flux to the surface was delivered by a variable power RF—excited CO_2 laser operating at 10.6 μm. The beam diameter was controlled by a combination of a fixed plano—concave lens and a movable plano—convex lens. Based on spectrophotometric measurements[12] the laser radiation at this wavelength was absorbed within 0.2 mm from the surface.

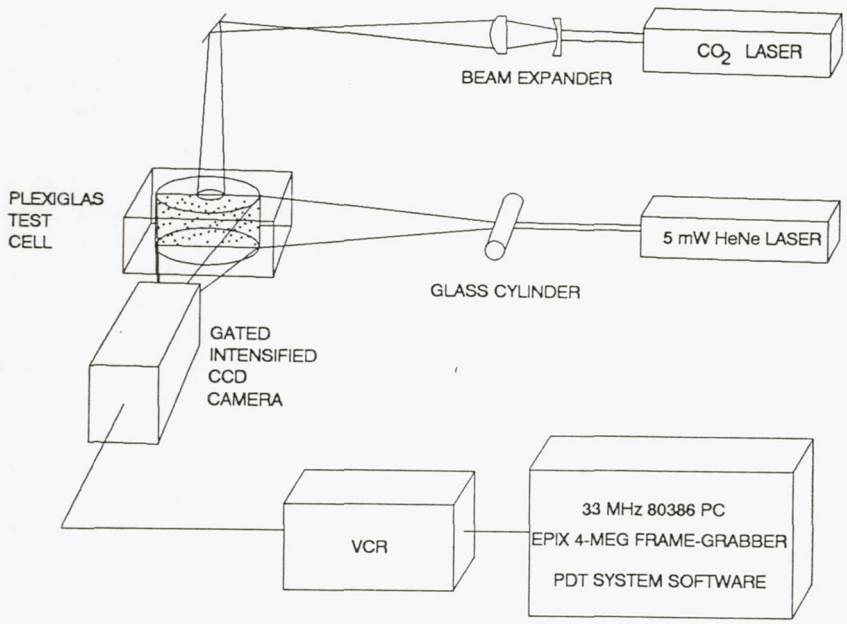

Figure 2. The STDCE ground—based experimental set—up showing the test cell, CO_2 laser and optics, HeNe flow visualization illumination laser, gated intensified CCD camera and the data reduction PC containing the EPIX 4—MEG video board and PDT software.

A 1 mm thick, 5 mW HeNe laser light sheet was used to illuminate a cross section of the test chamber. The HeNe laser light was scattered by 12 μm Pliolite particles. The scattered light was detected using a Xybion gated, intensified CCD camera with 768 × 493 pixels and recorded on a VHS videotape recorder. An Olympus 50—250 zoom lens operated at $f/11.0$ with a 7 mm extension tube was attached to the video camera using a C—mount to Olympus adapter. The camera gate time feature was essentially disabled yielding an exposure time of 16 ms. The camera gain was approximately 2/3 of the maximum. The 35 mm SLR camera, with the 50—250 zoom lens operated at $f/8.0$ and 46 mm of extension tubes, was mounted in place of the CCD camera after PDT data acquisition and used to make streak photographs of the flow.

3.2. Experimental technique

The particle concentration in the 10 centistoke kinematic viscosity silicone oil was adjusted manually in an iterative process until the PDT system detected approximately 600—800 particles per digitized video field. This was a compromise between too many particles, raising the number of false identifications, and too few data points. Although this process was qualitative, it is not difficult to reproduce (for the same hardware conditions), nor is it time consuming due to the near real time nature of the PDT system. The false identifications did not affect the correctness of the 'good' velocity vectors.

The data presented here consist of flow patterns resulting from a 20 mm heating beam diameter with a total power level of 1.20 W. The beam diameter was measured at the $1/e^2$ point. The actual power absorbed by the fluid was 90% of the beam power due to reflection at the liquid interface[12]. Therefore, the power level used in the numerical calculation was 1.02 W.

The raw video data for each run were acquired according to the following sequence. The CO_2 laser was energized and adjusted to the appropriate power level with the beam blocked. It was allowed to stabilize for approximately 30 minutes. Frequent measurements of the output power were used to confirm the stability. After the laser output was stable, the fluid/particle mixture was stirred to assure that the tracer particles were uniformly distributed. The VCR was then started at time t=0 and the CO_2 laser beam was unblocked, starting the flow. The resulting flow patterns were recorded for 45 minutes. The steady state wall temperature was also recorded as it was needed as an input for the numerical calculation.

The PDT data acquisition was started at t=24 minutes and lasted approximately 20 minutes. To insure the highest contrast and resolution images, data was acquired directly from the live video signal, but was also recorded in case additional data acquisition was needed and for archival purposes. One set of data was reacquired from the video tape because the original digitized images were inadvertently erased. The actual acquisition time for the longest IFT was 3.3 minutes; the majority of the time was used to store the 25 video fields to the PC hard disk. After the PDT data acquisition the CCD camera was replaced by the 35 mm SLR and 10 streak photographs were taken with different time exposures.

4. RESULTS AND DISCUSSION

4.1. Data acquisition and reduction

The method of digitizing the raw video data is a function of the characteristics of the flow. The dynamic range of the flow and whether the flow is transient or steady are important factors which dictate how the data are to be acquired. If the flow has a very high dynamic range the raw video data must be sampled using vastly different IFT's in order to capture both the slow and fast velocities. If the flow is steady, the acquisition of data with different IFT's can be done sequentially as the flow is time invariant. If the flow is transient one must be careful to use the same raw data (i.e. the same section of video tape) for the acquisition of each IFT to insure that the flow patterns change as little as possible during this time period. For the data presented here, the sampling times consist of IFT's of 5, 10, 20, 40, 60, 80, 120, 160, 240, 320, 480, all acquired sequentially over a 20 minute period. The above sampling provides a maximum possible dynamic range of 960:1.

The first step in processing the data is to determine the threshold level required to provide unique, non—overlapping particle images. This consists of setting all pixels under the selected threshold values to zero providing a black background. This level is high enough to eliminate camera noise from the image. The level chosen was grey level 45 out of 256. The boundaries of the chamber were determined so that only the active flow area was used during processing, eliminating an electronic date/time stamp and stray light caused by spurious reflections. This step also helps decrease the processing time. Figures 3 and 4 illustrate images with threshold values of 0 (unthresholded) and 45. Note that only the active area of the flow is shown.

A single program was written to perform both the boundary processing and the PDT tracking[11] for all 11 IFT's in a serial mode. Only the file names, threshold values and active flow areas are needed. The total processing time (both boundary processing and PDT tracking), including disk access and CPU time was 8.2 minutes to produce 2874 velocity vectors.

4.2. Experimental results and comparison with numerical calculation

The resulting velocity vector data from the 11 IFT's were combined to yield a high dynamic range velocity field. The raw velocity vector data are shown in Figure 5, plotted in nondimensional coordinates, where the radius, r/R is 0 to 1 and the height, z/Z is 0 to 1. Before plotting, the vectors were sorted to facilitate removal of duplicates (vectors with the same location), eliminating the smaller magnitudes. As shown in the figure a certain number of false velocity vectors exist due to random particle locations which satisfy the PDT algorithm. In Figure 5, 4.9% (140/2874) are false identifications, which is typical for this procedure, as reported in Reference 8.

Next an algorithm was used to eliminate the false identifications. The magnitude and direction of the 10 nearest neighbors to each velocity vector are used to test whether a certain vector is a false identification. In the algorithm two tests are performed. The mean speed of the flow was computed and compared to the vector in question; if the vector was greater than three times the mean, it was eliminated. The direction of the vector in question was compared to the standard deviation of the flow direction of the 10 nearest neighbors; if it differed by greater than one standard deviation, the vector was eliminated. Figure 6 shows the resulting velocity vector field after the application of this algorithm. 718 vectors were eliminated, reducing the false identifications to 1.1% (23/2093). The results for the detected vector magnitudes were accurate to 1.7% for the highest velocities

and 18% for the lowest velocities while the angular error ranges were 1.0 and 10.0 degrees respectively.

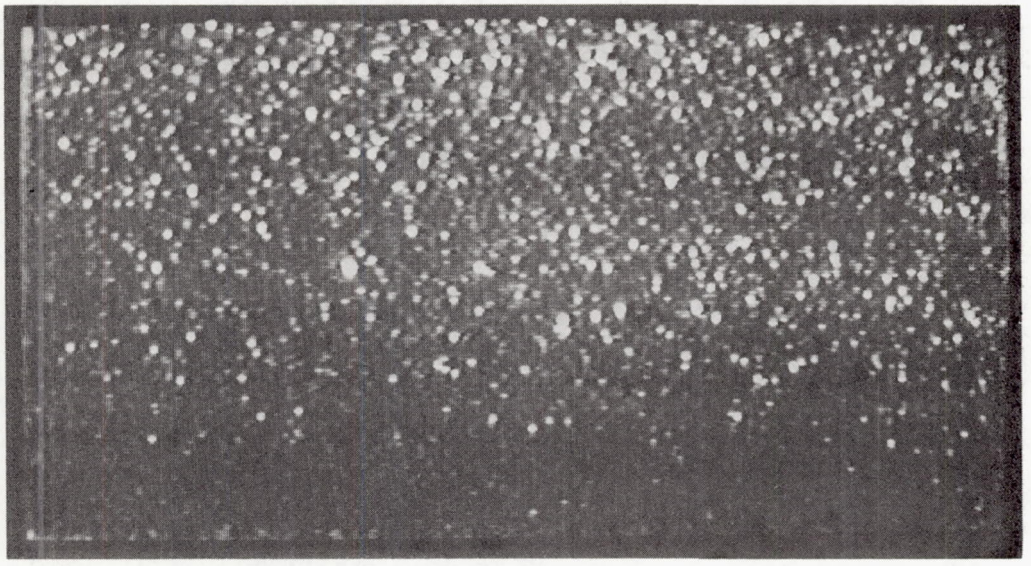

Figure 3. A sample unthresholded video field captured using the EPIX 4—MEG frame—grabber. Note that only the active area of the flow is shown.

Because the velocity vectors found are at random locations, an interpolation algorithm is used to produce velocity vector fields with data on a regular grid and to provide a velocity estimates in regions of sparse data. A linear least squares interpolation algorithm which utilizes the velocity vector information of the nearest twenty neighbors to the grid point in question accomplishes this task. A Gaussian smoothing filter is then passed over

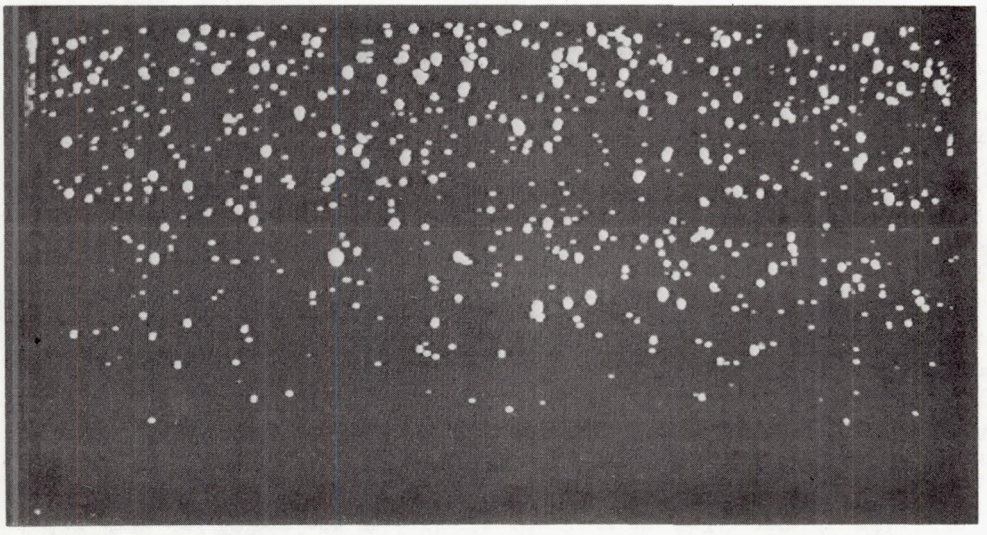

Figure 4. A sample video field captured using the EPIX 4—MEG frame—grabber, thresholded using a grey level of 45. Note that only the active area of the flow is shown.

the interpolated data. The algorithm allows for interpolation in a sub—region of the entire flow field to accommodate situations where there are stagnant regions of the flow field. In the case presented here, the flow is thermally stratified, and therefore contained within the top one half of the field below the free surface. In the interpolated plot shown in Figure 7, only the top 45% was used by the algorithm. This region was picked by observing the flow on the video tape and determining the active portion of the flow.

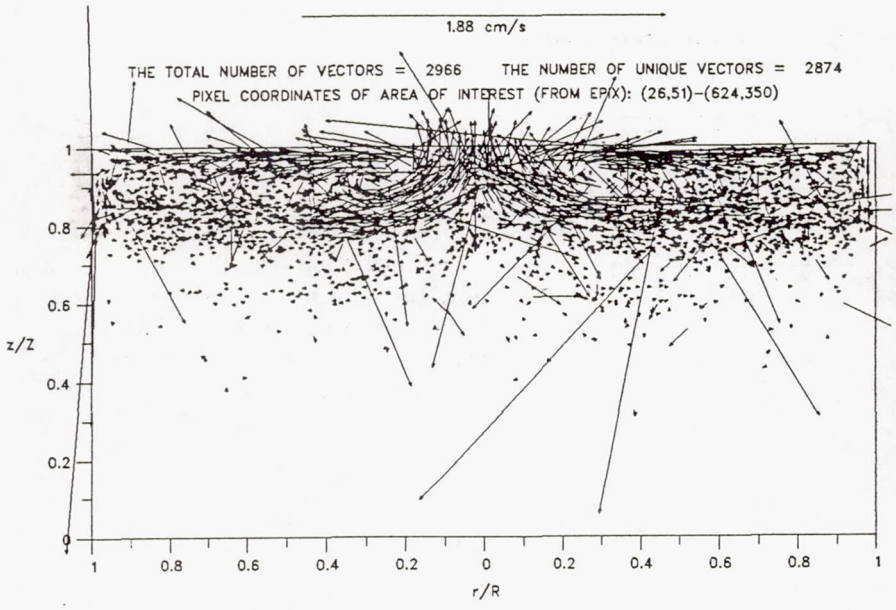

Figure 5. Raw two—dimensional velocity vectors plotted in normalized coordinates. The fluid surface is at z/Z=1 and the laser is incident at r/R=0, z/Z=1. 2966 vectors were found, but were reduced to 2874 after removal of duplicates. The reference scale in the figure represents the largest particle displacement found. 4.9% of the vectors were false identifications. Note the largest vector found corresponds to a false identification.

The interpolated data was used to compute the stream function. The streamlines for this flow are shown in Figure 8, plotted with 21 contour levels. The positive stream function values (solid lines) show the counter—clockwise rotating cell and the negative values (dotted lines) represent the clockwise rotating cell.

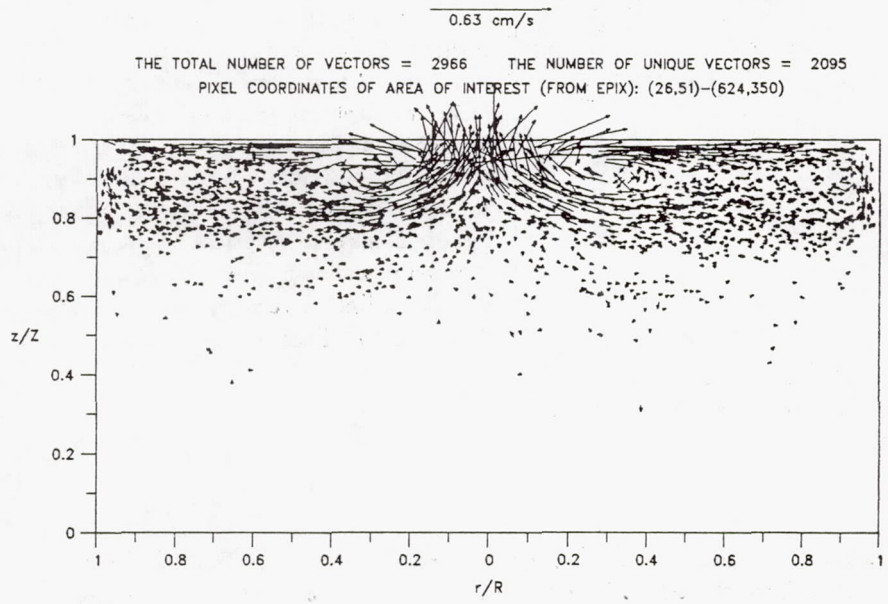

Figure 6. Two dimensional velocity vector data shown in Figure 5 after removal of the false identifications. 781 vectors were removed reducing the false identifications to 1.2%.

The first step in comparing the experimental and numerical techniques was to examine the streak photograph shown in Figure 9, as it was a direct record of the flow streamlines. This provided a good, credible benchmark for the flow structure. Then the PDT system data and the numerical data were compared to each other and to the benchmark streak photograph to illustrate and resolve any discrepancies.

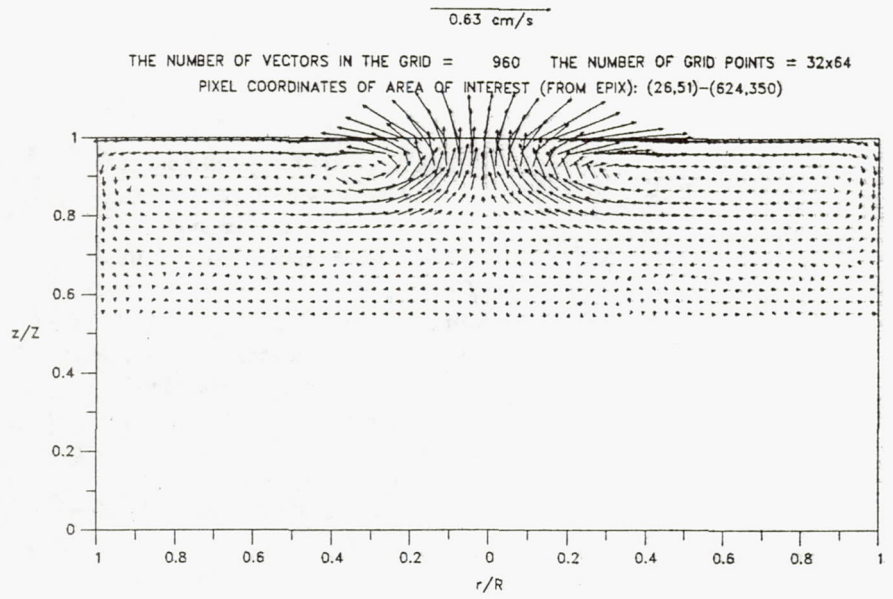

Figure 7. A 32×64 interpolated two—dimensional velocity field produced from the data in Figure 6. Note that the stagnant region of the flow, below z/Z=0.55 was not included in the interpolation calculation.

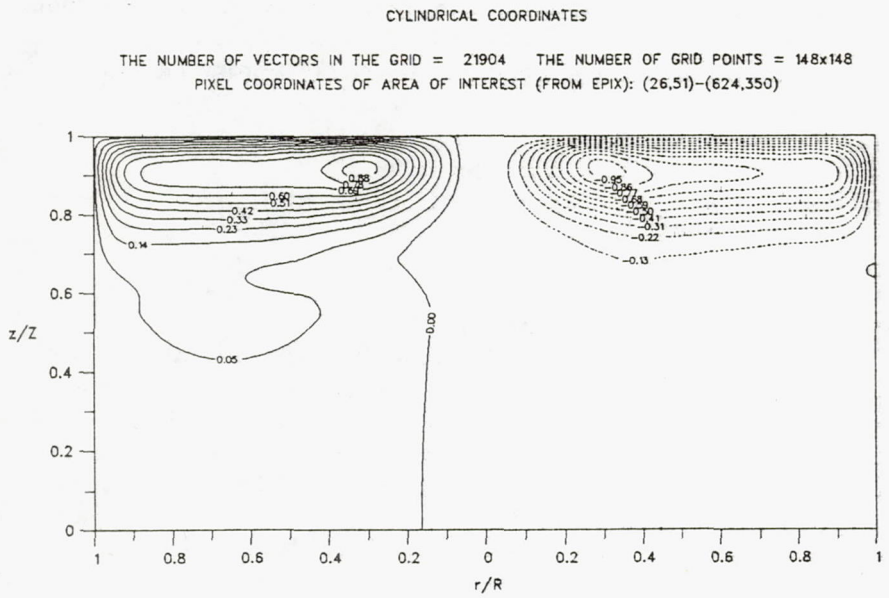

Figure 8. The stream function calculated from the PDT system data using a 148×148 interpolated grid showing the two counter rotating cells, but not the very slow secondary cells located below the main cells as indicated in Figures 6, 7, 8. The solid stream lines denote counter—clockwise rotation, while the dotted streamlines denote clockwise rotation. Several streamlines shown below the main cells are attributed to incomplete raw data. The streamline values are normalized to ±1.

The streak photograph (Figure 9) is a 22 second exposure which is equivalent to an IFT of 330, roughly capturing the same range of velocities in the flow as the PDT system data. These streaklines when compared to the stream function derived from the PDT system data (Figure 8) and the stream function from the numerical calculation (Figure 10) all show the same global flow structure; the symmetrical counter rotating cells. The location of the cell centers are all nearly in the same locations and are shown in Table 1.

The secondary cells below the main cells in Figures 8 and 9 do not show closure as is indicated by the calculated stream function in Figure 10. Experimentally, the cells reach outward close to the wall. This is supported by both the streak picture and the PDT system raw data shown in Figure 6. Neither a long enough

streak exposure nor a large enough IFT could be practically used to capture the slow velocities near the wall, which close the secondary cells. The particle settling velocities in this region were of the same order of magnitude as the flow velocities and would have distorted the data. Without data to show closure of the cells and the fact that the stream function values in this region are on the order of the noise in the calculation, the contouring algorithm did not draw streamlines for the secondary cells. None the less, the experimental data in Figure 6 shows substantially larger secondary cells. In addition, the lowest value streamlines in the main cells in Figure 10 penetrate deeply into the test chamber. No velocities were measured in this region using the PDT technique. Also, the streak photograph did not show any motion in the lower half of the flow field. The dynamic range in the calculated flow field is an order of magnitude greater ($\simeq$10,000:1) than the PDT system data, which allows for the measurement of velocities ten times slower, as the maximum measured and calculated

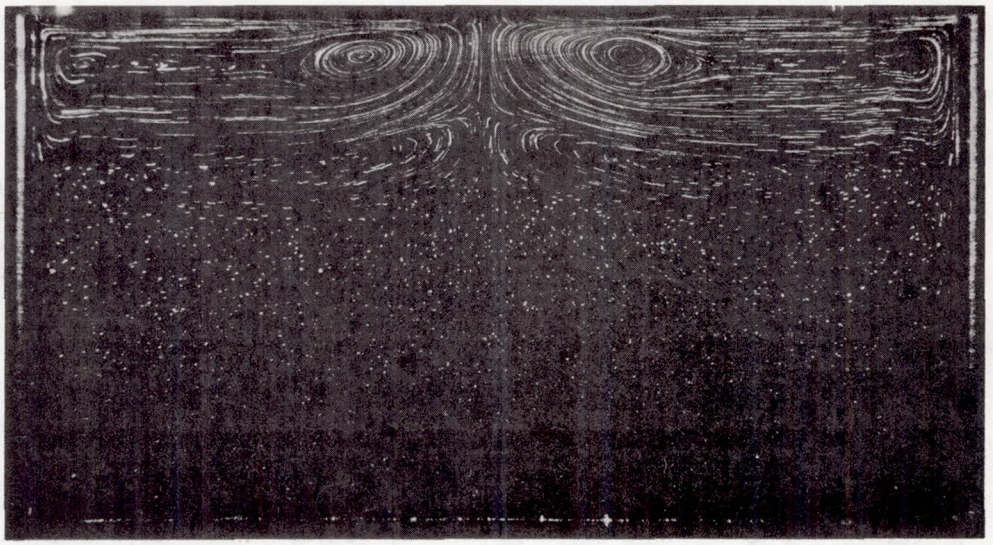

Figure 9. Streak photography illustrating the actual streamlines in the flow. The time exposure was 22 seconds, which was equivalent to an IFT of 330, capturing roughly the same flow velocities as the PDT system data.

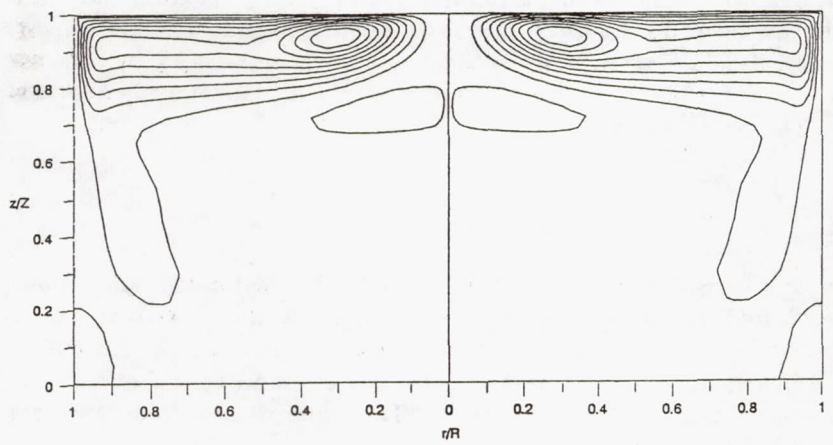

Figure 10. The stream function from the numerically calculated flow field using a 62×123 grid with the grid points concentrated at the walls, free surface and centerline (r/R$\simeq$0). The same number of contours are plotted as the experimental data shown in Figure 8.

velocities are roughly the same order. This was not seen in the experimental data for the aforementioned reason of not being able to obtain unbiased estimates of these low flow velocities.

A dip in the stream function near the wall and more compact streamlines are observed in the streak picture and in the numerical calculation. The numerical calculation has grid points clustered near the boundaries, allowing for high resolution near the wall. As a result the stream function is better defined in the region of high grid point density. The maximum grid of 148×148 used with the PDT system data could not provide this resolution, therefore, the plotted streamlines are slightly farther apart. The dip in the stream function at the side wall was not observed in the PDT stream function because the data in this region was too sparse to resolve this feature.

technique	left cell		right cell	
	r/R	z/Z	r/R	z/Z
PDT system data	0.31	0.92	0.31	0.92
streak photo	0.27	0.90	0.27	0.90
numerical calculation	0.31	0.94	0.31	0.94

Table 1. Comparison of flow cell centers for the experimental and numerical techniques.

A feature which is unique to the numerical data is the high acceleration of the outward flowing surface layer near the side wall. This phenomena was not observed in the PDT data nor in the streak photograph. The numerical calculation predicts this velocity spike at the wall due to a high temperature difference between the cold wall and the warmer surface fluid. The fact that the velocity spike was not observed experimentally indicates there may be a discrepancy between the modeled and actual side wall boundary condition.

Observation of the velocity vectors in Figure 6, shows that in the region r/R≃0.05–0.30 there are few velocity vectors. This is a result of three factors. Based on qualitative observation the particle images in this region tended to disappear in this high velocity region, eliminating the possibility of tracking them. The frame rate of the camera was too slow (1/60 sec) allowing too large a particle displacement between fields. The flow in this region was sharply accelerating (both magnitude and direction) violating the PDT system assumption of quasi–steady, linear flow during acquisition of each five–field set of images. Therefore, the measured maximum velocity of 0.63 cm/s was lower than the calculated velocity by a factor of 2. A higher measured velocity in this region would tend to pull the streamlines closer together in this region, moving the cell centers inward.

5. CONCLUSIONS

The PDT system was successful in producing velocity vector fields, which represent the physical flow. The false identification rate was reduced from 4.9% to 1.2% with the the application of comparative algorithm, without user intervention. Interpolated velocity vector fields were determined using a linear least squares routine to estimate the velocities in regions of sparse data and to plot the data on a regular grid. The stream function was calculated from the interpolated velocity field. The entire process from the start of the data acquisition tc the final plots took approximately $\frac{1}{2}$ hour.

The experimental stream function was compared to both a numerical calculation and a streak photograph under the same conditions. The results show that the PDT system faithfully represented the

physical flow. Some discrepancies were found and attributed to the limitations of the tracer particle images disappearing/reappearing in the high acceleration regions near the free surface, the limitations of the 1/60 second standard video field rate and the PDT system software assumption of nonaccelerating, linear flow during a five field sequence of acquired images. Overall, the discrepancies were minor considering the ease of use, low hardware complexity and cost of the system.

6. REFERENCES

1. S. Ostrach, "Convection Due to Surface Tension Gradients," *COSPAR Space Research*, Vol. 19, M.J. Rycroft, ed., 1979, pp. 563–570

2. Ch.–H. Chun and W. Wuest, "Experiments on the transition from the steady to oscillatory Marangoni convection of a floating zone under reduced gravity effect," *Acta Astronautica*, Vol. 6, 1979, p. 1073

3. Y. Kamotani and K. J. Lee, "Oscillatory Thermocapillary Flow in a Liquid Column Heated by a Ring Heater," *PCH Journal*, Vol. 11, No. 5/6, 1989, pp. 729–736

4. R. J. Adrian, "Multipoint Optical Measurements of Simultaneous Vectors in Unsteady Flow– A Review," *International Journal of Heat and Fluid Flow*, Vol. 7, 1986, pp. 127–145

5. L. Lourenco and A. Krothapalli, "Particle Image Displacement Velocimetry Measurements of a Three Dimensional Jet," *Physics of Fluids*, Vol. 31, 1988, pp. 1835–1837

6. R. Hoecker and J. Kompenhans, "Applications of Particle Image Velocimetry to Transonic Flows," 5th International Symposium on Applications of Laser Anemometry to Fluid Mechanics," Lisbon, Port., Paper #15.1, 1990

7. M. P. Wernet, "Two dimensional particle displacement tracking in particle image velocimetry," *Applied Optics*, Vol. 30, No. 14, 1991, pp. 1839–1846

8. M. P. Wernet and A. Pline, "Particle Image Velocimetry for the Surface Tension Driven Convection Experiment," Proceedings of the 4th International Conference on Laser Anemometry Advances and Applications, August 5–9, 1991

9. M. P. Wernet, "A New Data Reduction Technique for Pulsed Laser Velocimetry," PhD. Thesis, Case Western Reserve University, May 1989

10. K. C. Hsieh and A. Pline, "A Comprehensive Numerical Study of Surface Tension Driven Convection with Free Surface Deformation," 26th AIAA Thermophysics Conference, June 24–27, 1991, Paper # AIAA–91–1306

11. M. P. Wernet, "Software Manual for Operating Particle Displacement Tracking Data Acquisition and Reduction System," NASA TM 103720, January 1991

12. A. Pline, T.P. Jacobson, J.S. Wanhainen and D.A. Petrarca, "Hardware Development for the Surface Tension Driven Convection Experiment," *Journal of Spacecraft and Rockets*, 27, No. 23, 312–317, 1990

REPORT DOCUMENTATION PAGE

Form Approved
OMB No. 0704-0188

1. AGENCY USE ONLY (*Leave blank*)	2. REPORT DATE	3. REPORT TYPE AND DATES COVERED
		Technical Memorandum

4. TITLE AND SUBTITLE
Ground-Based PIV and Numerical Flow Visualization Results From the Surface Tension Driven Convection Experiment

5. FUNDING NUMBERS
WU 694 - 03 - 00

6. AUTHOR(S)
Alexander D. Pline, Mark P. Wernet, and Kwang-Chung Hsieh

7. PERFORMING ORGANIZATION NAME(S) AND ADDRESS(ES)
National Aeronautics and Space Administration
Lewis Research Center
Cleveland, Ohio 44135 - 3191

8. PERFORMING ORGANIZATION REPORT NUMBER
E - 6468

9. SPONSORING/MONITORING AGENCY NAMES(S) AND ADDRESS(ES)
National Aeronautics and Space Administration
Washington, D.C. 20546 - 0001

10. SPONSORING/MONITORING AGENCY REPORT NUMBER
NASA TM - 107172

11. SUPPLEMENTARY NOTES
Prepared for the 36th Annual International Symposium on Optical and Optoelectronic Applied Science and Engineering sponsored by the Society of Photo-Optical Instrumentation Engineers, San Diego, California, July 21-26, 1991. Alexander D. Pline, and Mark P. Wernet, NASA Lewis Research Center. Kwang-Chung Hsieh, Sverdrup Technology, Inc., Lewis Research Center Group, 2001 Aerospace Parkway, Brook Park, Ohio 44142 (work funded by NASA Contract NAS3-25266). Responsible person, Alexander D. Pline, (216) 433 - 6614.

12a. DISTRIBUTION/AVAILABILITY STATEMENT
Unclassified - Unlimited
Subject Category 35

12b. DISTRIBUTION CODE

13. ABSTRACT (*Maximum 200 words*)

The Surface Tension Driven Convection Experiment (STDCE) is a Space Transportation System flight experiment to study both transient and steady thermocapillary fluid flows aboard the USML—1 Spacelab mission planned for June, 1992. One of the components of data collected during the experiment is a video record of the flow field. This qualitative data is then quantified using an all electronic, two dimensional Particle Image Velocimetry (PIV) technique called Particle Displacement Tracking (PDT) which uses a simple space domain particle tracking algorithm. Results using the ground-based STDCE hardware, with a radiant flux heating mode, and the PDT system are compared to numerical solutions obtained by solving the axisymmetric Navier Stokes equations with a deformable free surface. The PDT technique is successful in producing a velocity vector field and corresponding stream function from the raw video data which satisfactorily represents the physical flow. A numerical program is used to compute the velocity vector field and corresponding stream function under identical conditions. Both the PDT system and numerical results were compared to a streak photograph, used as a benchmark, with good correlation.

14. SUBJECT TERMS
Marangoni convection; Particle trajectories; Velocity measurement

15. NUMBER OF PAGES
14

16. PRICE CODE
A03

17. SECURITY CLASSIFICATION OF REPORT	18. SECURITY CLASSIFICATION OF THIS PAGE	19. SECURITY CLASSIFICATION OF ABSTRACT	20. LIMITATION OF ABSTRACT
Unclassified	Unclassified	Unclassified	